Probabilistic Seasonal Outlook of the Rainy Season over Southeast Asia by Monitoring Its Onset

VASUBANDHU MISRA,[a,b,c] ALICE BRENNAN,[a,b,c] C. B. JAYASANKAR,[b,c] JOANNA RODGERS,[a,b,c] AND AMARJEET[b,d]

[a] *Department of Earth, Ocean and Atmospheric Science, Florida State University, Tallahassee, Florida*
[b] *Center for Ocean-Atmospheric Prediction Studies, Florida State University, Tallahassee, Florida*
[c] *Florida Climate Institute, Florida State University, Tallahassee, Florida*
[d] *Center for Ocean, River, Atmosphere, and Land Sciences (CORAL), Indian Institute of Technology Kharagpur, Kharagpur, India*

(Manuscript received 18 July 2024, in final form 1 June 2025, accepted 25 July 2025)

ABSTRACT: The Southeast Asian summer rainy season (SEASuRS) exhibits significant interannual variations, which are a challenge for reliable seasonal prediction. In this study, we provide a complementary approach to existing methodologies for the seasonal outlook of SEASuRS based on observational monitoring of the onset of the wet season. The onset and demise dates of SEASuRS are objectively diagnosed from the first and the last days of the year when the daily rain rates exceed the annual mean climatological rainfall at the granularity of the rainfall analysis. An ensemble of diagnosed onset/demise dates is generated by perturbing the original time series of observed daily rain rates to account for uncertainty at meso- to synoptic scales so that rain events unconnected to the annual cycle do not significantly influence the diagnosis of these dates. Our study shows that the interannual variations in the start dates of SEASuRS are significantly associated with variations in the season's length and seasonal rainfall. These local relationships are leveraged to generate probabilistic seasonal forecasts, which reveal that longer and wetter seasons associated with early onset or shorter and drier seasons associated with late onset seasons yield very skillful seasonal outlooks at the granularity of the available rainfall analysis.

SIGNIFICANCE STATEMENT: This work leverages the relationship of the onset date variations of the Southeast Asian summer rainy season (SEASuRS) to provide a probabilistic seasonal outlook of the forthcoming season. These seasonal outlooks of the wet season are based on the diagnosis of the onset dates from observed rainfall analysis. We find that an early or later onset of the wet season is closely associated with a longer and wetter or shorter and drier wet season, respectively. We generate an ensemble of seasonal outlooks by perturbing the original time series of daily rain rates to account for uncertainty in observations and in the diagnosis of the onset dates from random precipitation events that may be unconnected to the annual cycle of the rainfall. These ensembles of seasonal outlooks for the SEASuRS show significant skill, especially for anomalous seasons, and are suggested as a complementary approach to existing seasonal prediction techniques, especially when teleconnections with external signals like the ENSO and Indian Ocean dipole are relatively weak. Given the high population density and significant socioeconomic dependence on agriculture such seasonal outlooks could be extremely useful to mitigate the impacts of seasonal climate variability.

KEYWORDS: Climate prediction; Nowcasting; Seasonal forecasting; Climate variability; Interannual variability; Seasonal variability

1. Introduction

The large-scale Asian monsoon is broadly classified into three regional components: the South Asian, Southeast Asian, and East Asian monsoons (Lau and Li 1984; Krishnamurti 1985; Tao and Chen 1987; Lau and Yang 1997). In comparison to the other two regional components of the Asian monsoon, the climate variability of the Southeast Asian summer monsoon (SEAM) has received the least attention despite its considerable socioeconomic contribution to the region and globally (Lau and Yang 1997; Kripalani and Kulkarni 1997; Sen Roy and Kaur 2000). For example, SEAM is known for its vast tropical forests, which make up 15% of the world's tropical forests, has a very dense population with 8.5% of the world's population living in under 3% of Earth's total area, and is highlighted as one of the world's biodiversity hotspots (Sodhi et al. 2010; Stibig et al. 2014; Zheng et al. 2021).

Chronologically, the onset of SEAM occurs earliest in the year followed by the onset of the East Asian monsoon and then the onset of the South Asian monsoon (Tao and Chen 1987; Lau and Yang 1997; Wang and LinHo 2002; Zhang et al. 2004). Misra and DiNapoli (2014) indicate that SEAM has the longest wet season in the Asian monsoon region with its early onset. It should be noted that the monsoon season in addition to being featured by abrupt changes in daily rain rates (e.g., Tao and Chen 1987; Lau and Yang 1997; Matsumoto 1997; Wu and Zhang 1998) is also characterized by changes in

Supplemental information related to this paper is available at the Journals Online website: https://doi.org/10.1175/MWR-D-24-0148.s1.

Corresponding author: Vasubandhu Misra, vmisra@fsu.edu

DOI: 10.1175/MWR-D-24-0148.1

other thermodynamic and dynamic quantities like changes in precipitable water, ocean–land thermal contrast, and atmospheric circulation (Murakami and Ding 1982; He et al. 1987; Yanai et al. 1992; Webster et al. 1998; Zhang et al. 2004). However, this study follows from Misra and DiNapoli (2014), which diagnoses the onset and demise of the season based solely on daily rain rates. Therefore, we will hereafter refer to it as the Southeast Asian summer rainy season (SEASuRS). It may be noted that there is significant overlap between the SEAM season and SEASuRS.

The onset of SEASuRS occurs during the midboreal spring to early summer season, coinciding with the "spring predictability barrier" in the tropics (Webster and Yang 1992; Lau and Yang 1996). According to Lau and Yang (1997), SEAM is the sole large-scale convective system that occurs during the boreal spring season and has the potential to influence global climate variation. The interannual variations of SEAM are significantly higher than those of the other components of the Asian monsoon (Misra and DiNapoli 2014; Loo et al. 2015). Such interannual variations of SEAM can have a significant socioeconomic impact on the region (Lin et al. 2022; Ruiz-Barradas and Nigam 2018; Zhang et al. 2021). A strong monsoon could result in devastating floods, while a weak monsoon could be associated with droughts that can affect the livelihoods and economy of one of the most densely populated regions of the planet and could also exacerbate water insecurity issues in the region (Ruiz-Barradas and Nigam 2018; Zhang et al. 2021).

Misra and DiNapoli (2014) show that the major oceanic sources of moisture for SEASuRS are the Bay of Bengal, the Andaman Sea, the Gulfs of Martaban and Thailand, and the South China Sea. In years of a long SEAM season, the excess moisture sources in addition to the neighboring oceans also extend further westward from the western Indian Ocean. Misra and DiNapoli (2014) also indicate that years of SEASuRS with early onset are also associated with enhanced cross-equatorial flow and the Somali jet in the western Indian Ocean.

In this paper, we are expanding on the study of Misra and DiNapoli (2014) to provide a probabilistic seasonal outlook of SEASuRS by monitoring the onset of the season using NASA's Global Precipitation Measurement (GPM) product. It is widely recognized that Asian monsoon prediction is a challenge given the complexity of the interactions of ocean, land, and atmosphere (Webster et al. 1998; Wang et al. 2005; Liu et al. 2013; Jie et al. 2017). At the subseasonal and seasonal range, Jie et al. (2017) find that SEAM has the least skill in many of the operational models among the different regional components of the Asian monsoon. In this context, we are providing a complimentary methodology for the seasonal outlook of SEASuRS based solely on the monitoring of the onset of the season from observed rainfall analysis that can serve to supplement the existing operational practices for seasonal forecasting in the region.

2. Methodology and data

The methodology to objectively detect the onset and the demise of the rainy season follows from our earlier study (Misra et al. 2023). This methodology identifies the beginning and end dates of the rainy season as the first and last days of the year when the daily rainfall exceeds the annual mean climatological rainfall computed over the period of the dataset at every grid point of the rainfall analysis. To achieve this, we isolate the inflection points that appear as minima and maxima on the daily cumulative anomaly curve of rainfall, which are identified as the onset and demise dates of the season, respectively. There is a greater likelihood of misdiagnosing the onset/demise of the rainy season from random heavy precipitation events that are unconnected to the seasonal cycle since the diagnosis is done at individual grid points of the rainfall analysis. To overcome this limitation, this study uses the solution proposed in Misra et al. (2023) in which the original time series is perturbed 1000 times to develop an ensemble of estimates of the onset and demise dates of the rainy season. The perturbation is done by replacing the daily rainfall for a given day by randomly picking rainfall between −3 and +3 days to account for uncertainty in the meso–synoptic scales. It may be noted that many studies suggest that the precipitation features in the region are in the meso- to synoptic scales (e.g., Zipser et al. 2006; Liu and Zipser 2015). Therefore, a random rain event affecting the diagnosis of the onset/demise date from our methodology will appear with small likelihoods, while dates connected to the seasonal cycle will appear with higher probability in the ensemble spread. It should be mentioned that intraseasonal variations also contribute to the variations of the onset date (Wu and Wang 2000). This source of uncertainty, however, is not addressed in our current methodology of generating the ensemble members.

The daily rainfall data were sourced from the Integrated Multi-satellitE Retrievals for GPM, version 6 (IMERG; Huffman et al. 2019). The IMERG rainfall analysis is provided at a grid spacing of 0.1° (~10 km) with half-hourly temporal resolution spanning from June 2000 to the current date. Additionally, the IMERG data encompass rainfall analysis categorized as early, late, and final run products, each with a latency of approximately 4 h, 12 h, and 3.5 months, respectively. The latency of these products is determined by the time it takes to ingest data, preprocess the satellite radiances collected by the GPM, the analysis technique used, and the availability of atmospheric reanalysis products for the final release of the gridded rainfall product (Huffman et al. 2019). The methodology introduced in this study for diagnosing the evolution of the rainy season is also being adapted for real-time monitoring. Therefore, we have opted to utilize the 12-h latency product of IMERG. This choice allows for real-time application without compromising accuracy, while also benefiting from additional preprocessing compared to the 4-h latency product.

We also make use of the North American Multimodel Ensemble (NMME; Kirtman et al. 2014) seasonal hindcast for comparing our methodology of seasonal outlook with contemporary dynamical seasonal prediction. The seasonal hindcast from the NMME models is available for 1982–2010 (29 years) at a nominal grid spacing of 1° × 1°. We made use of monthly mean instead of the daily rainfall as this was available for all models and over the entire seasonal hindcast period. We also made use of a few recent years of their operational seasonal

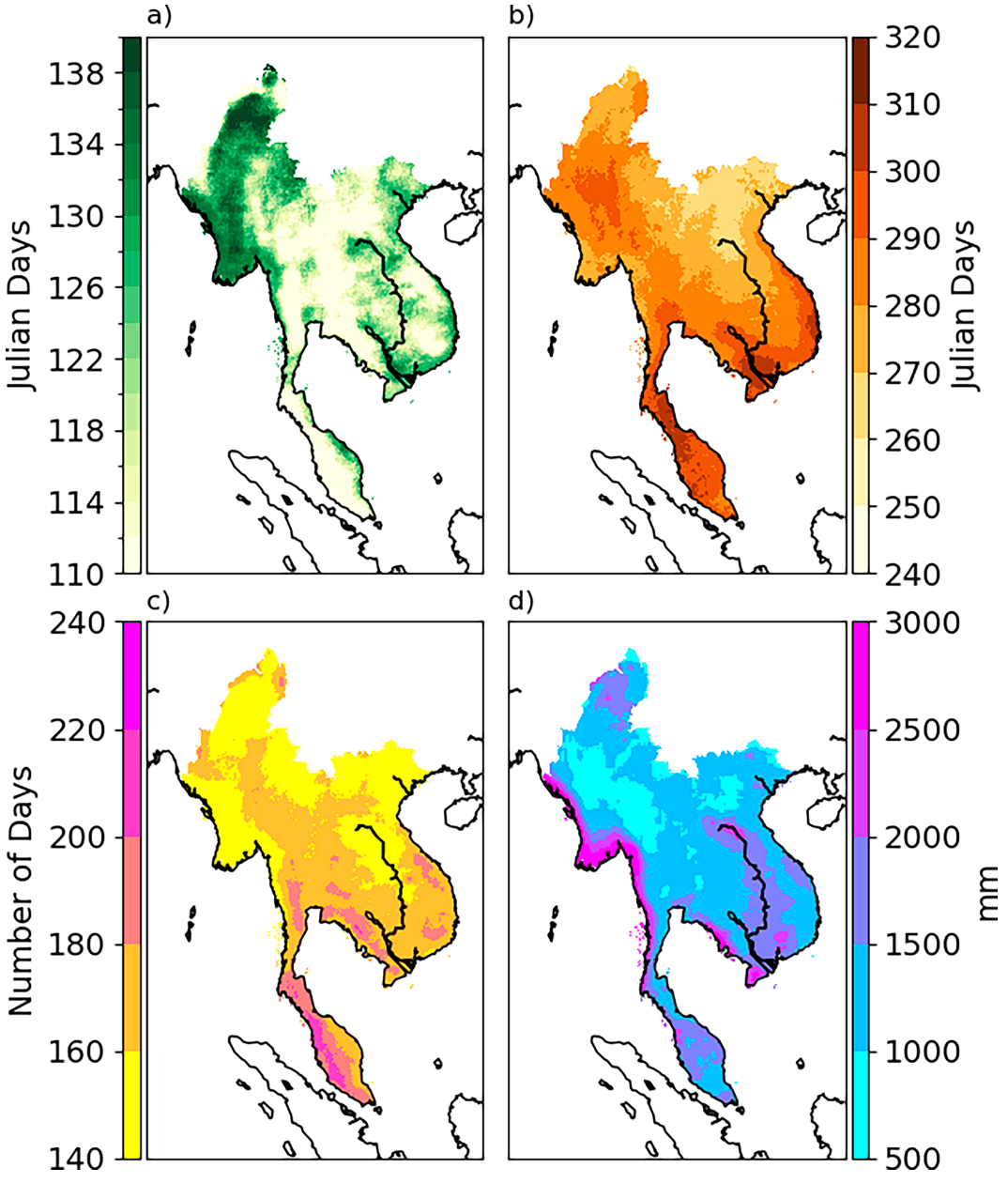

FIG. 1. The climatological median (a) start date (Julian day), (b) demise date (Julian day), (c) seasonal length (days), and (d) seasonal rain (mm) from the 12-h latency IMERG product. The climatology is computed over a 22-yr (2001–22) period of the dataset.

forecast products. To verify the rainfall of the NMME over the seasonal hindcast period, we used the rainfall analysis from Climate Hazards Group Infrared Precipitation with Stations (CHIRPS; Funk et al. 2015), available on a 0.5° grid over land surface only.

The domain of the analysis is shown in Fig. 1. The domain includes the countries of Myanmar, Thailand, Cambodia, Laos, Vietnam, and peninsular Malaysia. The SST dataset from Optimum Interpolation SST, version 2.1 (OISST2; Huang et al. 2021), available at 0.5° grid spacing at daily intervals is also used to diagnose the teleconnections of the Southeast Asian rainfall with

1) ENSO index: seasonally averaged SST over the Niño-3.4 region.
2) Indian Ocean dipole (IOD) index: seasonally averaged SST gradient between the western Indian Ocean (50°–70°E and 10°S–10°N) and eastern Indian Ocean (90°–110°E and 0°–10°S).

In addition, we also use upper-air variables from the fifth generation ECMWF atmospheric reanalysis (ERA5; Hersbach et al. 2020).

The ERA5 variables are used to examine the evolution of some dynamic and thermodynamic variables over the evolution of the SEASuRS. These variables include precipitable water, vertically integrated moisture flux, and a large-scale atmospheric stability parameter (γ) following Cook and Seager (2013), which is given by

$$\gamma = \pi_{\text{surf}} - \pi^*_{700}, \tag{1}$$

where π_{surf} is the surface moist static energy and π^*_{700} is the saturated moist static energy at 700 hPa. Cook and Seager (2013) explain that the difference in moist static energy (MSE) between a rising parcel of air from the surface, which becomes saturated at the lifting condensation level, and the saturated MSE at a specific altitude—typically above the boundary layer, around 700 hPa—is closely related to the thermal buoyancy of the parcel at that height. When the moist static energy of a rising, saturated parcel surpasses that of the surrounding environment, the parcel experiences positive buoyancy, creating an unstable atmospheric column, which initiates convection and precipitation.

All temporal correlations in this study are tested for false discovery rates on account of conducting statistical significance on all grid locations simultaneously following Benjamini and Hochberg (1995) and Ventura et al. (2004). This is done so by adjusting the p value to control the false rejection of the null hypothesis (i.e., false discovery rate) given the number of grid points where the hypothesis is tested. By controlling the false rejection of the null hypothesis, we can increase the confidence in the significance of our findings. According to this test, if the p value at a given grid point falls at or below the corresponding critical p value (p_{FDR}) as given below, then the grid point is said to pass the significance test:

$$p_{\text{FDR}}(i) = \frac{k}{M}\alpha, \tag{2}$$

where k is the rank order of the p value of grid point i, M is the total number of grid points, and α is the desired level of significance (which, in our case, is 0.05).

3. Results

a. Climatology

The climatology of the median value from the ensemble spread for onset and demise dates, corresponding seasonal length, and rainfall of SEASuRS is shown in Figs. 1a–d. The earliest onset dates of SEASuRS are in the western edge of the Malaysian Peninsula followed by peninsular Thailand and regions in the east including over Laos, Cambodia, and Vietnam, which range from approximately 90 to 120 Julian days (Fig. 1a). The latest onset dates of the rainy season are over Myanmar, where the onset dates range beyond 130 Julian days (Fig. 1a). The corresponding evolution of the composite precipitable water, moisture flux, and γ [Eq. (1)] around the time of the onset (~Julian day 110) is shown in Fig. S1 in the online supplemental material. This figure shows the gradual northward progression of higher precipitable water, accompanied by increased dominance of the southwesterly moisture flux and a significant increase in large-scale instability as the onset date is approached and thereafter.

Similarly, in Fig. 1b, the last demise dates (≥200 Julian days) of SEASuRS are largely over the western edge of the Malaysian Peninsula and along coastal and some interior parts of Thailand, Cambodia, and Vietnam. However, the earliest demise dates are over most of Myanmar and northern parts of the rest of the SEAM region (Fig. 1b). The corresponding evolution of the composite precipitable water, moisture flux, and γ around the demise date (~Julian day 270) in Fig. S2 shows that the high precipitable water and southwesterly moisture flux recede southward as the large-scale instability reduces. In fact, over the Malaysian Peninsula and parts of Indonesia, the westerly moisture flux transitions to easterly moisture flux, thereby maintaining the precipitable water and large-scale instability in the region.

The climatological onset and demise date distributions of SEASuRS then give rise to very long rainy seasons (ranging between 290 and 310 days) over the peninsulas of Malaysia and Thailand and along the coastal regions of Thailand, Cambodia, and Vietnam (Fig. 1c). In contrast, the length of the rainy season is comparatively shorter (<290 days) over Myanmar and in the rest of the interior regions (Fig. 1c). Interestingly, the climatological seasonal rainfall over this rainy season is highest along the Myanmar coast followed by the Mekong basin region, the Malaysian Peninsula, and along coastal Vietnam and Cambodia. This indicates that daily rain rates over some of these regions are dictating the higher seasonal rains in some of these regions despite the shorter rainy season compared to some of the other regions indicated in Fig. 1c.

b. Interannual variations

The corresponding standard deviations of the onset, demise, length, and seasonal rainfall of the rainy season are shown in Figs. 2a–d, respectively. Generally, the stronger variations shown in Fig. 2 are coincident with earlier onset dates, later demise dates, longer seasonal lengths, and higher seasonal rains in Fig. 1. For example, the Malaysian Peninsula exhibits some of the largest variations in the onset (Fig. 2a) and demise (Fig. 2b) dates in the region with the least over the Myanmar coast. The rest of the SEAM region shows a relatively high variation of onset dates of 15–30 days (Fig. 2a), while the variability of the demise dates is comparatively lower (10–15 days; Fig. 2b). Therefore, the variability of the length of the wet season across the region is in the range of about 30 days with peninsular Malaysia showing even larger variations of nearly 45–50 days (Fig. 2c). The variability of the seasonal precipitation is largest along the coastal regions including peninsular Malaysia and the Mekong River basin, while in the rest of the domain it is nearly 5 times less (Fig. 2d).

We also examined the signal-to-noise ratio (see section S1 for description) of the four parameters shown in Fig. 1. A higher value of this ratio (>1) for a given parameter suggests the dominance of the signal, and in this context, it would mean that it is more strongly tied to the seasonal cycle or other low-frequency variations. In contrast, a lower value of

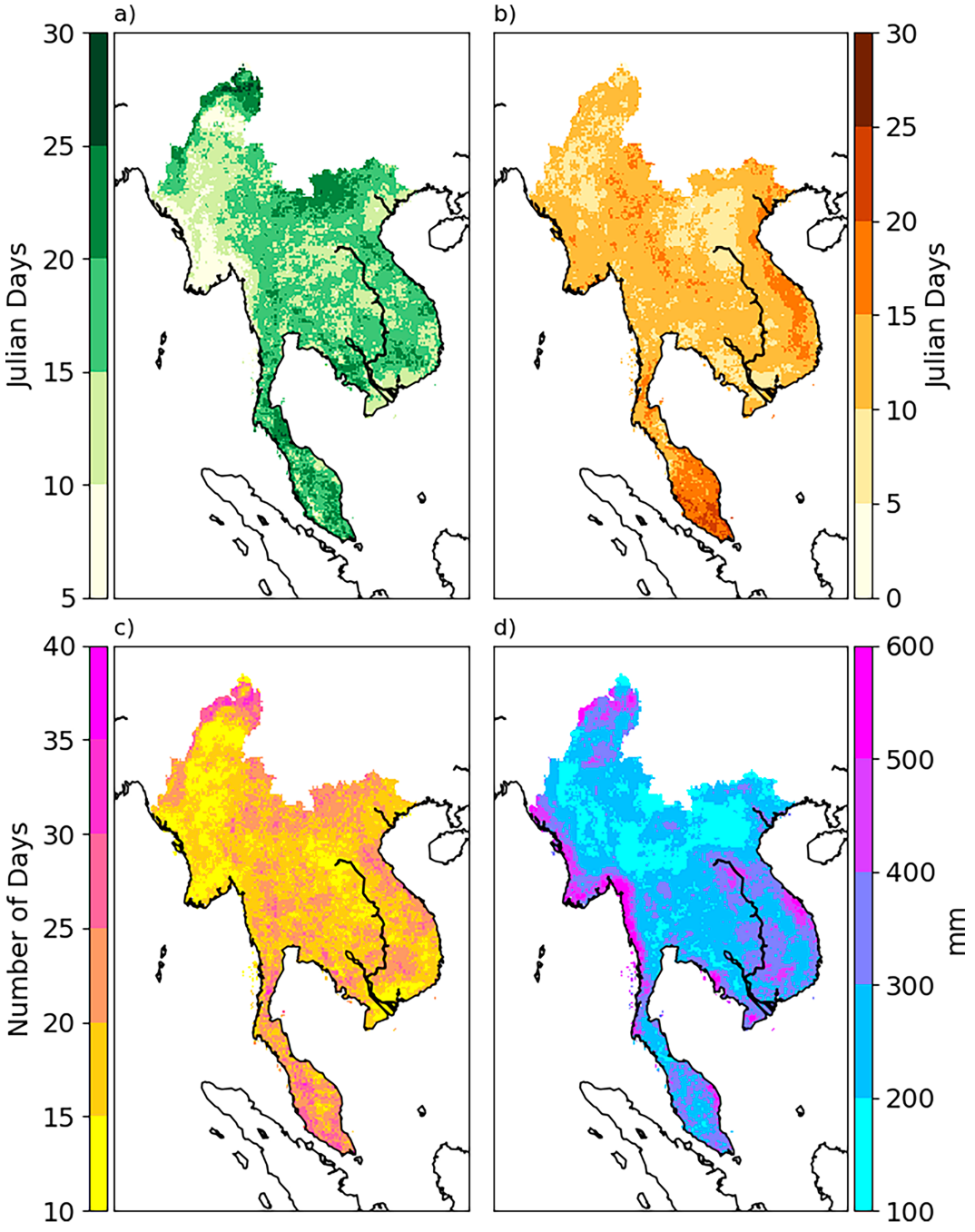

FIG. 2. The standard deviation of (a) start date (days), (b) retreat date (days), (c) length (days), and (d) seasonal rain (mm) of the wet season.

the signal-to-noise ratio (<1) would imply that noise dominates which means that the random synoptic-to-mesoscale rain events are more likely to determine the diagnosis of the given parameter of the SEASuRS. These ratios are shown using the 1001 ensemble members of the time series at each grid point for the onset date (Fig. 3a), demise date (Fig. 3b), seasonal length (Fig. 3c), and seasonal rainfall (Fig. 3d). In the case of the onset date variations, the signal-to-noise ratio is low (<1) in the valleys and plains and higher (>1) near orographic and coastal regions (Fig. 3a). However, the signal-to-noise ratio is comparatively higher for the demise date especially over the broad region of the Mekong River basin (Fig. 3b), while the distribution of the signal-to-noise ratio for the seasonal length in Fig. 3c is between those in Figs. 3a and 3b. Interestingly, the signal-to-noise ratio for the seasonal rainfall is the highest among all the other SEASuRS parameters with the

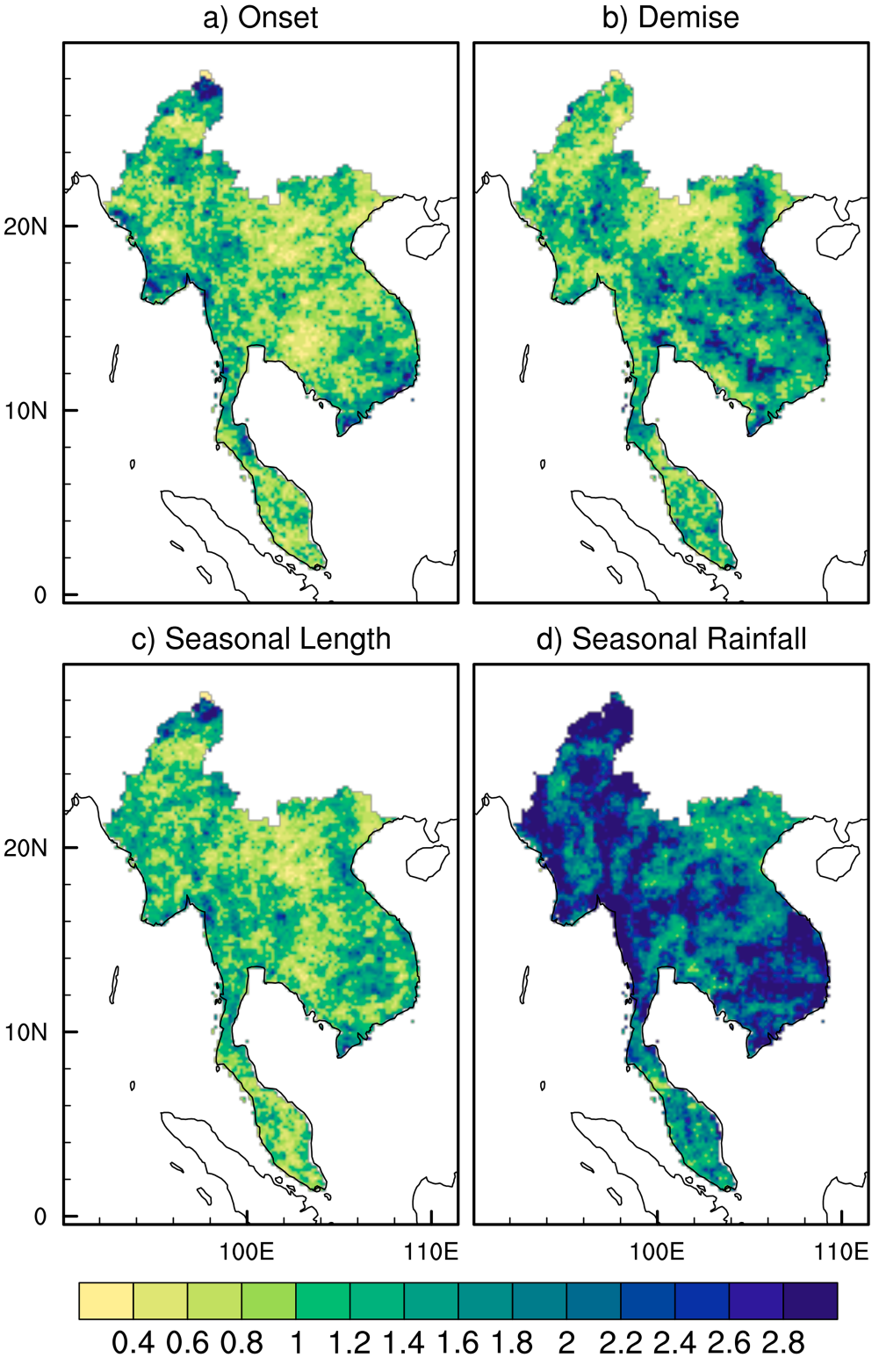

FIG. 3. The signal-to-noise ratio for (a) onset date, (b) demise date, (c) seasonal length, and (d) seasonal rainfall from the 1001 ensemble members.

ratio well over 1.0 (Fig. 3d). Given these results in Fig. 3, there is some hope for seasonal predictability of the seasonal rainfall, while the predictability of the onset date of SEASuRS is going to be the most challenging followed by that for the seasonal length.

The local variability of SEASuRS is further illustrated by the correlations of its onset date variations with its seasonal length and rainfall as shown in Figs. 4a and 4b, respectively. A robust relationship is observed in these figures with the implication that in all of SEAM region, an early or later onset date of the wet season is associated with a longer and wetter or shorter and drier season, respectively. For example, the fractional coverage of significant correlations in Figs. 4a and 4b is 99% and 51.5%, respectively. Similarly, the correlations with the demise date suggest that a later or early demise is linked to a longer and wetter or shorter and drier wet season, respectively (Figs. 4c,d). In this instance, the fractional coverage of significant correlations in Figs. 4c and 4d is 84% and 41%, respectively. However, the relationship between the onset and demise date variations is comparatively weak and insignificant (not shown). It is interesting to note that the onset date has such robust relationships with the corresponding seasonal length and seasonal rainfall of SEASuRS despite their contrasting signal-to-noise ratios.

To contrast the local relationships shown in Fig. 4, we show the remote influence of ENSO variations on SEASuRS in Fig. S3. Although the correlations at some of the grid points in Fig. S3 pass the t test at the 95% confidence interval, they fail the Benjamini and Hochberg (1995) test for field significance suggesting that the ENSO teleconnection with the variations of the SEASuRS is weak and insignificant. Similarly, the correlations of SEASuRS with the preceding Niño-3.4 SST anomalies for the MAM season (Fig. S4) also fail the Benjamini and Hochberg (1995) test. It may be noted that the ENSO teleconnection with the rainfall in the region varies from month to month. For example, Yang et al. (2020) indicate that above-normal rainfall in May and July in the Indo-China Peninsula tends to occur at different stages of ENSO, which leads to a weaker relationship with the total summer seasonal rainfall anomaly. Likewise, the contemporaneous correlations of the SON seasonal mean IOD index with demise date, length, and seasonal rain of SEASuRS also fail the Benjamini and Hochberg (1995) test (Fig. S5). Many of the earlier studies that suggested strong correlations of ENSO and IOD were related to SEAM (e.g., Kripalani and Kulkarni 1997; Saji and Yamagata 2003; Hamada et al. 2012; Amirudin et al. 2020), in contrast to SEASuRS of this study. Furthermore, none of the earlier studies conducted any field significance test on these teleconnections to confirm their robustness.

It is clear from comparing Figs. S3–S5 that the remote forcing on SEASuRS is not as statistically robust and strong as the local relationships shown in Fig. 4. This relatively weaker remote forcing on SEAM further makes the challenges of seasonal prediction in the region stiff (Singhrattna et al. 2005; Shrivastava et al. 2017). The complex orography, robust land–atmosphere, and air–sea interactions prevalent in the region give rise to significant internal variations (Meehl 1994; Wang et al. 2005; Misra 2008; Liu et al. 2014; Shrivastava et al. 2017; Xavier et al. 2014). However, in this study, we suggest that the local relationships indicated in Fig. 4 could be leveraged to supplement the existing efforts of seasonal climate prediction in the region. For example, by monitoring the variations of the onset date in real time could yield a seasonal outlook (Misra et al. 2022, 2023). This is attempted in the context of SEASuRS in the following subsection.

c. *Seasonal outlooks of the wet season*

The availability of IMERG rainfall in near–real time makes it possible to operationally monitor the onset date of SEASuRS. The evolution of the cumulative anomaly curve of rainfall day by day could be monitored, and the date of the relative minima in the curve could be marked as the onset date of the wet season. However, operationally, the minima in the cumulative anomaly curve of the rainfall are detected after the fact, usually within a week of the onset date. This delay, although undesirable, is necessary to confirm the local minima in the cumulative anomaly curve of the daily rainfall, which is critical to yield a reliable seasonal outlook of SEASuRS. Based on the local relationships shown in Fig. 4 and with the generation of 1000 ensemble members, we can make probabilistic forecasts for the seasonal outlook of the wet season. The probabilistic skill score of the area under the relative operating characteristic curve (AUROC) is used here to assess the skill of this seasonal outlook based on the anomalies of the onset date of SEASuRS. AUROC is a commonly used assessment metric with scores ≥ 0.5 considered to be more skillful than random forecasts (Stanski et al. 1989; WMO 2000; Graham et al. 2000). In Figs. 5a and 5b, we show the AUROC score for the likelihood of a longer season and a wetter season from an anomalously early start to the wet season (based on tercile thresholds), respectively. The AUROC scores are above 0.5, and in many regions across the SEAM region are over 0.8. Similarly, the AUROC scores for the probability of a shorter season and a drier season from a delayed onset of the wet season (based on tercile thresholds) are shown in Figs. 5c and 5d, respectively. Here, the AUROC scores are nearly 0.8 or higher across the domain, which is significantly higher than for early onset seasons. But AUROC scores for normal onset date seasons (in the middle tercile), although greater than 0.5 across the region (Figs. 5e,f), are, however, significantly less than those for the anomalous onset seasons. This is because this heuristic model for the seasonal outlook is based on the linear relationship between the onset date variations and the seasonal variations of the wet season, which is bound to produce the highest skills for the most anomalous seasons associated with anomalous onset dates.

4. Discussion

The proposed method to provide a seasonal outlook of the SEASuRS from monitoring its onset date is simple but effective. In the absence of strong teleconnections of the SEASuRS with the variations of tropical oceans, it is not surprising that Southeast Asia is a challenging region for seasonal prediction from climate models (Singhrattna et al. 2005; Shrivastava et al. 2017; Wang et al. 2015; Xing et al. 2016; Jie et al. 2017).

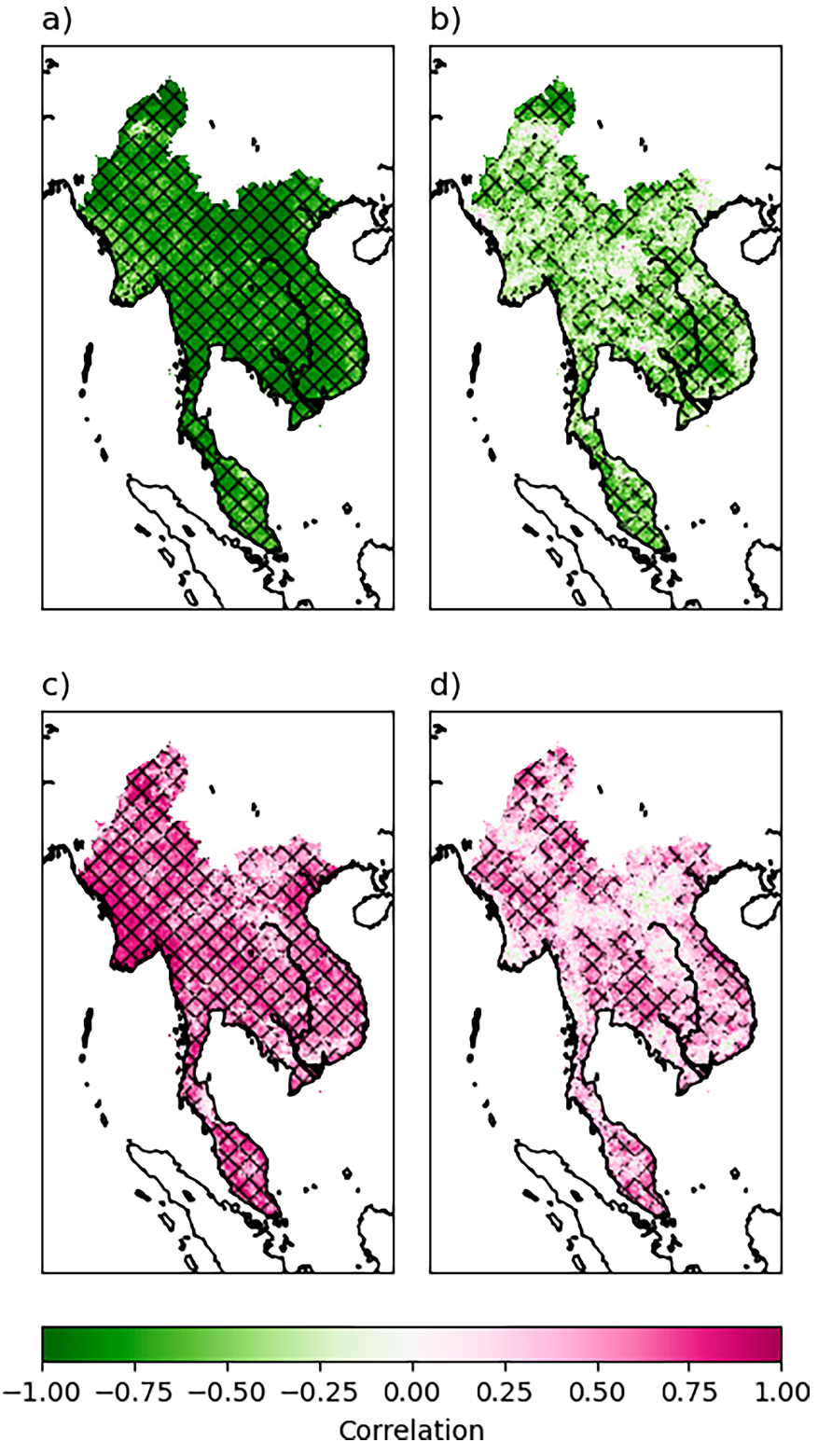

FIG. 4. The correlations of the anomalies of the median start date with anomalies of the median of (a) seasonal length and (b) seasonal rain of the wet season. Similarly, the correlations of the anomalies of the median demise date with anomalies of the median of (c) seasonal length and (d) seasonal rain. The crosshatching indicates statistical significance at the 5% significance level following the Benjamini and Hochberg (1995) test.

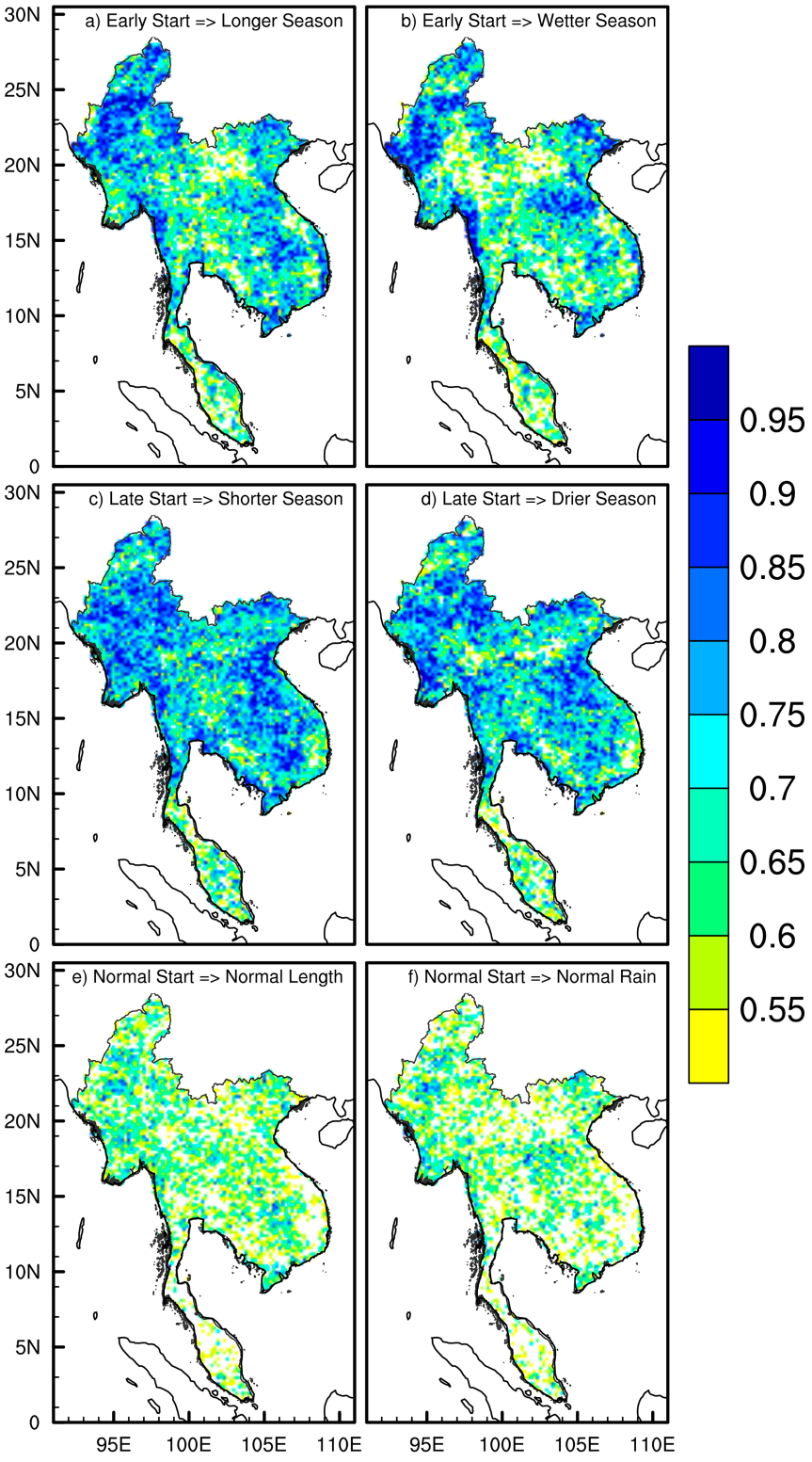

FIG. 5. The AUROC for the outlook of (a) a longer wet season and (b) a wetter wet season based on an early start, (c) a shorter wet season, and (d) a drier wet season based on the later start of the wet season, (e) a normal wet season length based on the normal start of the wet season, and (f) a normal wet season rainfall based on the normal start of the wet season. Only regions with AUROC ≥ 0.5, which signifies probabilistic skill better than a random forecast, are shaded.

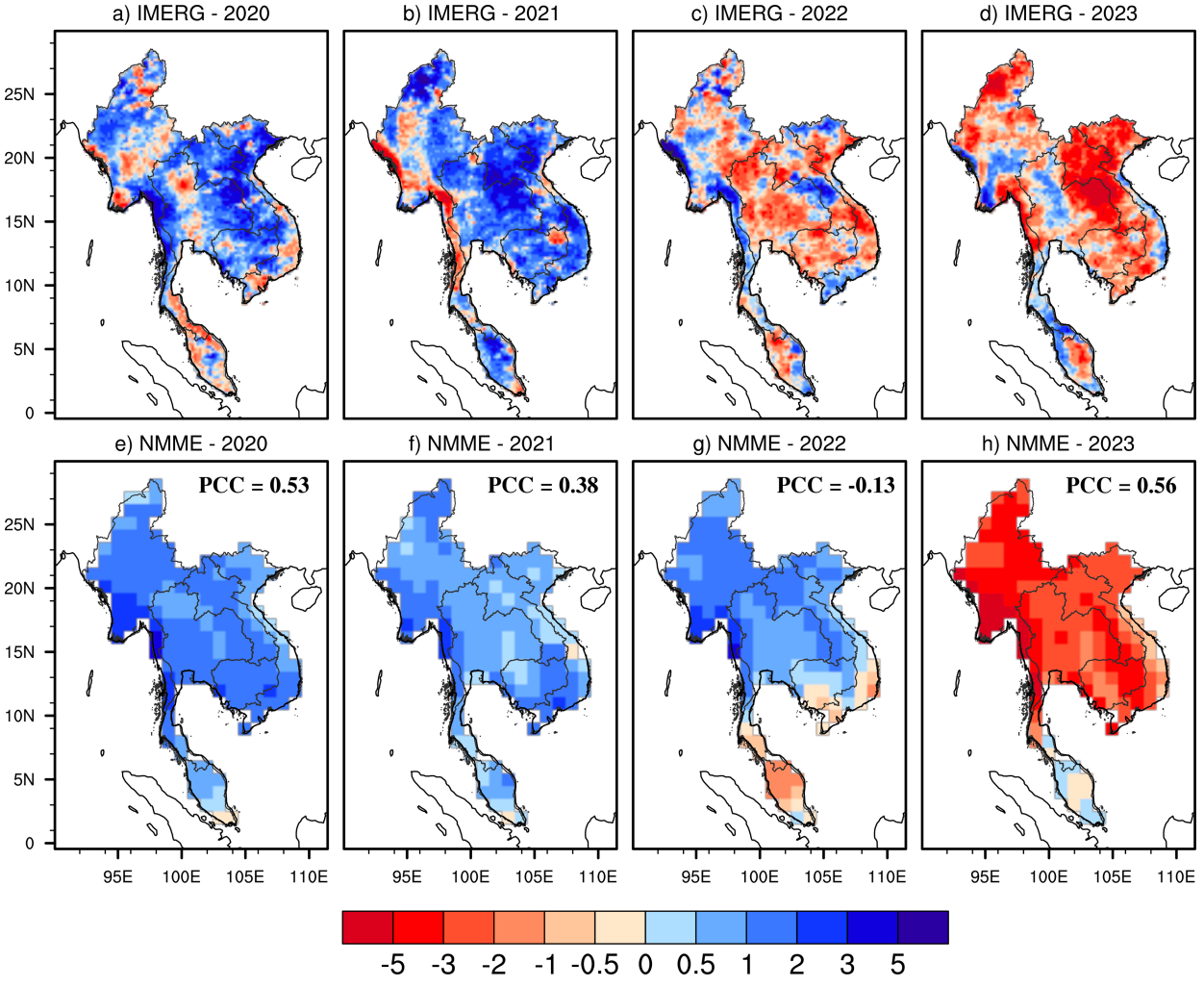

FIG. 6. The seasonal average precipitation anomalies (mm day^{-1}) for April–September from (a)–(d) IMERG and (e)–(h) NMME at zero lead time (April start) for (a),(e) 2020, (b),(f) 2021, (c),(g) 2022, and (d),(h) 2023. The pattern correlation coefficient (PCC) of each model with the corresponding IMERG seasonal anomalies is indicated in the top-right corner of (e)–(h).

We also illustrate the poor seasonal prediction skills at zero-month lead (with April start) for the April–September period (roughly the SEASuRS period) from the NMME (Kirtman et al. 2014) in Fig. 6. The NMME is a set of current state-of-the-art seasonal climate prediction models used operationally for seasonal forecasts by several organizations around the world including the Climate Prediction Center of NOAA.

In Fig. 6, we show the multimodel ensemble mean of the April–September seasonal rainfall anomalies for four recent years from five NMME models (GEOS5, GEMNEMO, CFSv2, CanCM4, and CCSM4) along with the corresponding IMERG observations for four recent seasons. The results in Fig. 6 are somewhat sobering with the verification of the multimodel rainfall anomalies appearing to be unreliable from year to year. The pattern correlations of the April–September mean rainfall anomalies for each of the years are indicated in each panel (Figs. 6e–h), which range from −0.13 to 0.56. A similar analysis is conducted for the individual models instead of the multimodel mean and is illustrated in Figs. S6 and S7, which indicate a further decrease in the pattern correlations relative to the multimodel mean in Fig. 6. Although these figures are not a comprehensive analysis of the performance of the NMME in the region, it does illustrate the findings of the earlier studies about the challenges of seasonal prediction over this region (e.g., Jiang et al. 2013; Singhrattna et al. 2005; Shrivastava et al. 2017; Kim et al. 2016; Roy et al. 2020).

Furthermore, the relatively observed weak teleconnections of the SEASuRS with ENSO and the IOD also contribute to the prospect for poor dynamical seasonal prediction skills in climate models. For example, the NMME models display inconsistent ENSO teleconnections with the SEASuRS compared to the corresponding observations (Fig. S8). In Fig. S8, we see that models like GEMNEMO, GEOS, and CanCM4 display spatially extensive contemporaneous correlations of Niño-3.4 SST anomalies with corresponding SEASuRS rainfall anomalies in contrast to the limited correlations seen over

the peninsular region in the observed panel. Similarly, models like CCSM4 or CFSv2 display almost nonexistent or weak teleconnections with the ENSO index that are also inconsistent with observations (Fig. S8). In addition, it may be noted that NMME models tend to erroneously amplify SST anomalies in the Niño-3.4 region (Larson and Kirtman 2017; Barnston et al. 2019; Tippett et al. 2019, 2020), which could further exacerbate some of these teleconnection biases in some specific years.

This study has highlighted the strong local relationships of the onset date with seasonal rainfall and the seasonal length of SEASuRS (Fig. 4) and their contrasting signal-to-noise ratios (Fig. 3). Given the relatively low signal-to-noise ratio of the onset date (Fig. 3a) and its strong relationships with the length and seasonal rainfall anomalies of SEASuRS, it raises a challenge for dynamical seasonal prediction over the region. Therefore, it is not surprising to note the limited seasonal predictability displayed by NMME over this region as the seasonal variability is dependent on these local relationships that are not necessarily influenced by large-scale external forcing. Moreover, NMME models, which have been extensively applied over various regions of the globe, are also noted for their biases (Slater et al. 2017, 2019; Yazdandoost et al. 2020; Teshome et al. 2022), which are consistent with some of our findings here. Therefore, in light of these results, we claim that a simple monitoring of the evolution of the onset of SEASuRS can lead to reliable seasonal outlooks for Southeast Asia that will be complimentary to the current efforts. The simplicity of the proposed approach in this study is its strength.

5. Conclusions

The Southeast Asian monsoon (SEAM) seasonal climate variability is significant and one of the largest in the Asian monsoon domain. These large seasonal climate variations coupled with high population density and significant socioeconomic development in the region necessitate a reliable seasonal climate prediction for the region. There are still considerable challenges to predicting variations of SEAM despite the well-known influences of ENSO and IOD variations on SEAM. This is partially because of the complex interactions between land, ocean, and atmosphere that give rise to considerable local and internal variability. In this study, we leverage the inherent local relationships to provide seasonal outlooks of the Southeast Asian summer rainy season (SEASuRS).

We introduced a robust method to define the onset and demise of SEASuRS by perturbing the rainfall time series 1000 times using IMERG rainfall analysis data. With the availability of high-resolution rainfall data like IMERG, this methodology can be easily and effectively adapted for real-time monitoring of the wet season's evolution in the region. We show that a useful probabilistic seasonal outlook of SEASuRS could be provided by the monitoring of its onset date. Since SEASuRS is solely based on daily rain rates, it could also include the premonsoon rainfall. However, the two seasons of SEASuRS and SEAM significantly overlap. We show that the onset date variations of SEASuRS are significantly correlated with its length and the seasonal rainfall variations across the region and are not dependent on its demise date variations. This relationship reveals that early or later onset seasons are associated with longer and wetter or shorter and drier wet seasons. These relationships appear to be stronger and statistically more significant than the teleconnections of SEASuRS with ENSO or IOD. These local variations of the wet season of SEAM with the onset date variations are leveraged to provide skillful seasonal outlooks of the wet season at the granularity of NASA's IMERG rainfall analysis (at 0.1° grid resolution). Amid weak teleconnections of SEASuRS with the variability of the tropical oceans, and its dependence on its onset date variations that have a comparatively low signal-to-noise ratio, the proposed methodology of the seasonal outlook from monitoring the onset date variations at the granularity of the rainfall analysis appears promising.

Acknowledgments. We acknowledge the support from NASA Grant 80NSSC22K0595. The IMERG dataset was provided by the NASA Goddard Space Flight Center and PPS which developed and computed the IMERG as a contribution to GPM and archived it at the NASA GES DISC.

Data availability statement. The IMERG rainfall data from NASA were obtained from https://gpm1.gesdisc.eosdis.nasa.gov/data/GPM_L3/. The SST dataset was obtained from https://psl.noaa.gov/data/gridded/data.noaa.oisst.v2.highres.html. The NMME hindcast dataset is available from https://www.ncei.noaa.gov/products/weather-climate-models/north-american-multi-model.

REFERENCES

Amirudin, A. A., E. Salimun, F. Tangang, L. Juneng, and M. Zhuairi, 2020: Differential influences of teleconnections from the Indian and Pacific Oceans on rainfall variability in Southeast Asia. *Atmosphere*, **11**, 886, https://doi.org/10.3390/atmos11090886.

Barnston, A. G., M. K. Tippett, M. Ranganathan, and M. L. L'Heureux, 2019: Deterministic skill of ENSO predictions from the North American Multimodel Ensemble. *Climate Dyn.*, **53**, 7215–7234, https://doi.org/10.1007/s00382-017-3603-3.

Benjamini, Y., and Y. Hochberg, 1995: Controlling the false discovery rate: A practical and powerful approach to multiple testing. *J. Roy. Stat. Soc.*, **57B**, 289–300, https://doi.org/10.1111/j.2517-6161.1995.tb02031.x.

Cook, B. I., and R. Seager, 2013: The response of the North American monsoon to increased greenhouse gas forcing. *J. Geophys. Res. Atmos.*, **118**, 1690–1699, https://doi.org/10.1002/jgrd.50111.

Funk, C., and Coauthors, 2015: The Climate Hazards Infrared Precipitation with Stations—A new environmental record for monitoring extremes. *Sci. Data*, **2**, 150066, https://doi.org/10.1038/sdata.2015.66.

Graham, R. J., A. D. L. Evans, K. R. Mylne, M. S. J. Harrison, and K. B. Robertson, 2000: An assessment of seasonal predictability using atmospheric general circulation models. *Quart. J. Roy. Meteor. Soc.*, **126**, 2211–2240, https://doi.org/10.1002/qj.49712656712.

Hamada, J.-I., S. Mori, H. Kubota, M. D. Yamanaka, U. Haryoko, S. Lestari, R. Sulistyowati, and F. Syamsudin, 2012: Interannual rainfall variability over northwestern Jawa and its relation to

the Indian Ocean Dipole and El Niño-Southern Oscillation events. *SOLA*, **8**, 69–72, https://doi.org/10.2151/sola.2012-018.

He, H., J. W. McGiness, Z. Song, and M. Yanai, 1987: Onset of the Asian summer monsoon in 1979 and the effect of the Tibetan Plateau. *Mon. Wea. Rev.*, **115**, 1966–1995, https://doi.org/10.1175/1520-0493(1987)115<1966:OOTASM>2.0.CO;2.

Hersbach, H., and Coauthors, 2020: The ERA5 global reanalysis. *Quart. J. Roy. Meteor. Soc.*, **146**, 1999–2049, https://doi.org/10.1002/qj.3803.

Huang, B., C. Liu, V. Banzon, E. Freeman, G. Graham, B. Hankins, T. Smith, and H.-M. Zhang, 2021: Improvements of the Daily Optimum Interpolation Sea Surface Temperature (DOISST) version 2.1. *J. Climate*, **34**, 2923–2939, https://doi.org/10.1175/JCLI-D-20-0166.1.

Huffman, G. J., D. T. Bolvin, E. J. Nelkin, and J. Tan, 2019: Integrated Multi-Satellite Retrievals for GPM (IMERG) technical documentation. IMERG Tech. Doc., 77 pp., https://gpm.nasa.gov/sites/default/files/document_files/IMERG_doc_190909.pdf.

Jiang, X., S. Yang, Y. Li, A. Kumar, X. Liu, Z. Zuo, and B. Jha, 2013: Seasonal-to-interannual prediction of the Asian summer monsoon in the NCEP Climate Forecast System version 2. *J. Climate*, **26**, 3708–3727, https://doi.org/10.1175/JCLI-D-12-00437.1.

Jie, W., F. Vitart, T. Wu, and X. Liu, 2017: Simulations of the Asian summer monsoon in the Sub-Seasonal to Seasonal Prediction Project (S2S) database. *Quart. J. Roy. Meteor. Soc.*, **143**, 2282–2295, https://doi.org/10.1002/qj.3085.

Kim, G., and Coauthors, 2016: Global and regional skill of the seasonal predictions by WMO Lead Centre for long-range forecast multi-model ensemble. *Int. J. Climatol.*, **36**, 1657–1675, https://doi.org/10.1002/joc.4449.

Kirtman, B. P., and Coauthors, 2014: The North American Multimodel Ensemble: Phase-1 seasonal-to-interannual prediction; phase-2 toward developing intraseasonal prediction. *Bull. Amer. Meteor. Soc.*, **95**, 585–601, https://doi.org/10.1175/BAMS-D-12-00050.1.

Kripalani, R. H., and A. Kulkarni, 1997: Rainfall variability over south–East Asia—Connections with Indian monsoon and ENSO extremes: New perspectives. *Int. J. Climatol.*, **17**, 1155–1168, https://doi.org/10.1002/(SICI)1097-0088(199709)17:11<1155::AID-JOC188>3.0.CO;2-B.

Krishnamurti, T. N., 1985: Summer Monsoon Experiment—A review. *Mon. Wea. Rev.*, **113**, 1590–1626, https://doi.org/10.1175/1520-0493(1985)113<1590:SMER>2.0.CO;2.

Larson, S. M., and B. P. Kirtman, 2017: Drivers of coupled model ENSO error dynamics and the spring predictability barrier. *Climate Dyn.*, **48**, 3631–3644, https://doi.org/10.1007/s00382-016-3290-5.

Lau, K.-M., and M.-T. Li, 1984: The monsoon of East Asia and its global associations—A survey. *Bull. Amer. Meteor. Soc.*, **65**, 114–125, https://doi.org/10.1175/1520-0477(1984)065<0114:TMOEAA>2.0.CO;2.

——, and S. Yang, 1996: The Asian monsoon and predictability of the tropical ocean–atmosphere system. *Quart. J. Roy. Meteor. Soc.*, **122**, 945–957, https://doi.org/10.1002/qj.49712253208.

Lau, K. M., and S. Yang, 1997: Climatology and interannual variability of the Southeast Asian summer monsoon. *Adv. Atmos. Sci.*, **14**, 141–162, https://doi.org/10.1007/s00376-997-0016-y.

Lin, H.-I., Y.-Y. Yu, F.-I. Wen, and P.-T. Liu, 2022: Status of food security in East and Southeast Asia and challenges of climate change. *Climate*, **10**, 40, https://doi.org/10.3390/cli10030040.

Liu, C., and E. J. Zipser, 2015: The global distribution of largest, deepest, and most intense precipitation systems. *Geophys. Res. Lett.*, **42**, 3591–3595, https://doi.org/10.1002/2015GL063776.

Liu, D., G. Wang, R. Mei, Z. Yu, and H. Gu, 2014: Diagnosing the strength of land–atmosphere coupling at subseasonal to seasonal time scales in Asia. *J. Hydrometeor.*, **15**, 320–339, https://doi.org/10.1175/JHM-D-13-0104.1.

Liu, X., S. Yang, A. Kumar, S. Weaver, and X. Jiang, 2013: Diagnostics of subseasonal prediction biases of the Asian summer monsoon by the NCEP Climate Forecast System. *Climate Dyn.*, **41**, 1453–1474, https://doi.org/10.1007/s00382-012-1553-3.

Loo, Y. Y., L. Billa, and A. Singh, 2015: Effect of climate change on seasonal monsoon in Asia and its impact on the variability of monsoon rainfall in Southeast Asia. *Geosci. Front.*, **6**, 817–823, https://doi.org/10.1016/j.gsf.2014.02.009.

Matsumoto, J., 1997: Seasonal transition of summer rainy season over Indochina and adjacent monsoon region. *Adv. Atmos. Sci.*, **14**, 231–245, https://doi.org/10.1007/s00376-997-0022-0.

Meehl, G. A., 1994: Influence of the land surface in the Asian summer monsoon: External conditions versus internal feedbacks. *J. Climate*, **7**, 1033–1049, https://doi.org/10.1175/1520-0442(1994)007<1033:IOTLSI>2.0.CO;2.

Misra, V., 2008: Coupled interactions of the monsoons. *Geophys. Res. Lett.*, **35**, L12705, https://doi.org/10.1029/2008GL033562.

——, and S. DiNapoli, 2014: The variability of the Southeast Asian summer monsoon. *Int. J. Climatol.*, **34**, 893–901, https://doi.org/10.1002/joc.3735.

——, C. B. Jayasankar, P. Beasley, and A. Bhardwaj, 2022: Operational monitoring of the evolution of rainy season over Florida. *Front. Climate*, **4**, 793959, https://doi.org/10.3389/fclim.2022.793959.

——, S. Dixit, and C. B. Jayasankar, 2023: The regional diagnosis of onset and demise of the rainy season over tropical and subtropical Australia. *Earth Interact.*, **27**, https://doi.org/10.1175/EI-D-22-0026.1.

Murakami, T., and Y.-H. Ding, 1982: Wind and temperature changes over Eurasia during the early summer of 1979. *J. Meteor. Soc. Japan*, **60**, 183–196, https://doi.org/10.2151/jmsj1965.60.1_183.

Roy, T., X. He, P. Lin, H. E. Beck, C. Castro, and E. F. Wood, 2020: Global evaluation of seasonal precipitation and temperature forecasts from NMME. *J. Hydrometeor.*, **21**, 2473–2486, https://doi.org/10.1175/JHM-D-19-0095.1.

Ruiz-Barradas, A., and S. Nigam, 2018: Hydroclimate variability and change over the Mekong River basin: Modeling and predictability and policy implications. *J. Hydrometeor.*, **19**, 849–869, https://doi.org/10.1175/JHM-D-17-0195.1.

Saji, N. H., and T. Yamagata, 2003: Possible impacts of Indian Ocean Dipole mode events on global climate. *Climate Res.*, **25**, 151–169, https://doi.org/10.3354/cr025151.

Sen Roy, N., and S. Kaur, 2000: Climatology of monsoon rains of Myanmar (Burma). *Int. J. Climatol.*, **20**, 913–928, https://doi.org/10.1002/1097-0088(20000630)20:8<913::AID-JOC485>3.3.CO;2-L.

Shrivastava, S., S. C. Kar, and A. R. Sharma, 2017: Inter-annual variability of summer monsoon rainfall over Myanmar. *Int. J. Climatol.*, **37**, 802–820, https://doi.org/10.1002/joc.4741.

Singhrattna, N., B. Rajagopalan, M. Clark, and K. Krishna Kumar, 2005: Seasonal forecasting of Thailand summer monsoon rainfall. *Int. J. Climatol.*, **25**, 649–664, https://doi.org/10.1002/joc.1144.

Slater, L. J., G. Villarini, and A. A. Bradley, 2017: Weighting of NMME temperature and precipitation forecasts across Europe. *J. Hydrol.*, **552**, 646–659, https://doi.org/10.1016/j.jhydrol.2017.07.029.

——, ——, and ——, 2019: Evaluation of the skill of North-American Multi-Model Ensemble (NMME) Global Climate Models in predicting average and extreme precipitation and temperature over the continental USA. *Climate Dyn.*, **53**, 7381–7396, https://doi.org/10.1007/s00382-016-3286-1.

Sodhi, N. S., M. R. C. Posa, T. M. Lee, D. Bickford, L. P. Koh, and B. W. Brook, 2010: The state and conservation of Southeast Asian biodiversity. *Biodiversity Conserv.*, **19**, 317–328, https://doi.org/10.1007/s10531-009-9607-5.

Stanski, H. R., L. J. Wilson, and W. R. Burrows, 1989: Survey of common verification methods in meteorology. WMO Tech. Rep. WMO/TD-358, 81 pp., https://www.cawcr.gov.au/projects/verification/Stanski_et_al/Stanski_et_al.html.

Stibig, H.-J., F. Achard, S. Carboni, R. Raši, and J. Miettinen, 2014: Change in tropical forest cover of Southeast Asia from 1990 to 2010. *Biogeosciences*, **11**, 247–258, https://doi.org/10.5194/bg-11-247-2014.

Tao, S., and L. Chen, 1987: A review of recent research on the East Asian summer monsoon in China. *Monsoon Meteorology*, C.-P. Chang and T. N. Krishnamurti, Eds., Oxford University Press, 60–92.

Teshome, A., and Coauthors, 2022: Skill assessment of North American Multi-Models Ensemble (NMME) for June-September (JJAS) seasonal rainfall over Ethiopia. *Atmos. Climate Sci.*, **12**, 54–73, https://doi.org/10.4236/acs.2022.121005.

Tippett, M. K., M. Ranganathan, M. L'Heureux, A. G. Barnston, and T. DelSole, 2019: Assessing probabilistic predictions of ENSO phase and intensity from the North American Multimodel Ensemble. *Climate Dyn.*, **53**, 7497–7518, https://doi.org/10.1007/s00382-017-3721-y.

——, M. L. L'Heureux, E. J. Becker, and A. Kumar, 2020: Excessive momentum and false alarms in late-spring ENSO forecasts. *Geophy Res Lett.*, **47**, e2020GL087008, https://doi.org/10.1029/2020GL087008.

Ventura, V., C. J. Paciorek, and J. S. Risbey, 2004: Controlling the proportion of falsely rejected hypotheses when conducting multiple tests with climatological data. *J. Climate*, **17**, 4343–4356, https://doi.org/10.1175/3199.1.

Wang, B., and LinHo, 2002: Rainy season of the Asian–Pacific summer monsoon. *J. Climate*, **15**, 386–398, https://doi.org/10.1175/1520-0442(2002)015<0386:RSOTAP>2.0.CO;2.

——, Q. Ding, X. Fu, I.-S. Kang, K. Jin, J. Shukla, and F. Doblas-Reyes, 2005: Fundamental challenge in simulation and prediction of summer monsoon rainfall. *Geophys. Res. Lett.*, **32**, L15711, https://doi.org/10.1029/2005GL022734.

——, B. Xiang, J. Li, P. J. Webster, M. N. Rajeevan, J. Liu, and K.-J. Ha, 2015: Rethinking Indian monsoon rainfall prediction in the context of recent global warming. *Nat. Commun.*, **6**, 7154, https://doi.org/10.1038/ncomms8154.

Webster, P. J., V. O. Magana, T. N. Palmer, J. Shukla, R. A. Tomas, M. Yanai, and T. Yasunari, 1998: Monsoons: Processes, predictability, and the prospects for prediction. *J. Geophys. Res.*, **103**, 14451–14510, https://doi.org/10.1029/97JC02719.

Webster, P. J., and S. Yang, 1992: Monsoon and ENSO: Selectively interactive systems. *Quart. J. Roy. Meteor. Soc.*, **118**, 877–926, https://doi.org/10.1002/qj.49711850705.

WMO, 2000: Standardized verification system (SVS) for long-range forecasts (LRF). WMO Attachment II.8, 17 pp., https://www.metoffice.gov.uk/binaries/content/assets/metofficegovuk/pdf/research/climate-science/climate-observations-projections-and-impacts/svslrf.pdf.

Wu, G., and Y. Zhang, 1998: Tibetan Plateau forcing and the timing of the monsoon onset over South Asia and the South China sea. *Mon. Wea. Rev.*, **126**, 913–927, https://doi.org/10.1175/1520-0493(1998)126<0913:TPFATT>2.0.CO;2.

Wu, R., and B. Wang, 2000: Interannual variability of summer monsoon onset over the western North Pacific and the underlying processes. *J. Climate*, **13**, 2483–2501, https://doi.org/10.1175/1520-0442(2000)013<2483:IVOSMO>2.0.CO;2.

Xavier, P., R. Rahmat, W. K. Cheong, and E. Wallace, 2014: Influence of Madden-Julian Oscillation on Southeast Asia rainfall extremes: Observations and predictability. *Geophys. Res. Lett.*, **41**, 4406–4412, https://doi.org/10.1002/2014GL060241.

Xing, W., B. Wang, and S.-Y. Yim, 2016: Peak-summer East Asian rainfall predictability and prediction part I: Southeast Asia. *Climate Dyn.*, **47**, 1–13, https://doi.org/10.1007/s00382-014-2385-0.

Yanai, M., C. Li, and Z. Song, 1992: Seasonal heating of the Tibetan Plateau and its effects on the evolution of the Asian summer monsoon. *J. Meteor. Soc. Japan*, **70**, 319–351, https://doi.org/10.2151/jmsj1965.70.1B_319.

Yang, Y., R. Wu, and C. Wang, 2020: Individual and combined impacts of tropical Indo-Pacific SST anomalies on interannual variation of the Indochina peninsular precipitation. *J. Climate*, **33**, 1069–1088, https://doi.org/10.1175/JCLI-D-19-0262.1.

Yazdandoost, F., S. Moradian, M. Zakipour, A. Izadi, and M. Bavandpour, 2020: Improving the precipitation forecasts of the North-American Multi Model Ensemble (NMME) over Sistan basin. *J. Hydrol.*, **590**, 125263, https://doi.org/10.1016/j.jhydrol.2020.125263.

Zhang, L., Z. Chen, and T. Zhou, 2021: Human influence on the increasing drought risk over Southeast Asian monsoon region. *Geophys. Res. Lett.*, **48**, e2021GL093777, https://doi.org/10.1029/2021GL093777.

Zhang, Z., J. C. L. Chan, and Y. Ding, 2004: Characteristics, evolution and mechanisms of the summer monsoon onset over Southeast Asia. *Int. J. Climatol.*, **24**, 1461–1482, https://doi.org/10.1002/joc.1082.

Zheng, Z., and Coauthors, 2021: Anthropogenic impacts on Late Holocene land-cover change and floristic biodiversity loss in tropical southeastern Asia. *Proc. Natl. Acad. Sci.*, **118**, e2022210118, https://doi.org/10.1073/pnas.2022210118.

Zipser, E. J., D. J. Cecil, C. Liu, S. W. Nesbitt, and D. P. Yorty, 2006: Where are the most intense thunderstorms on Earth? *Bull. Amer. Meteor. Soc.*, **87**, 1057–1072, https://doi.org/10.1175/BAMS-87-8-1057.

Supplementary Material

Probabilistic Seasonal Outlook of the Rainy Season over Southeast Asia by Monitoring its Onset

Vasubandhu Misra[1, 2, 3,#], Alice Brennan[1, 2, 3], C. B. Jayasankar[2, 3], Joanna Rodgers[1, 2, 3], & Amarjeet[2, 4]

[1]Department of Earth, Ocean and Atmospheric Science, Florida State University, Tallahassee, Florida, U. S. A.

[2]Center for Ocean-Atmospheric Prediction Studies, Florida State University, Tallahassee, Florida, U. S. A.

[3]Florida Climate Institute, Florida State University, Tallahassee, Florida, U. S. A.

#Corresponding Author: vmisra@fsu.edu

[4]Center for Ocean, River, Atmosphere, and Land Sciences (CORAL), Indian Institute of Technology Kharagpur, Kharagpur, India

S1 Computing Signal to Noise Ratio

We compute the signal-to-noise ratio of the four quantities (onset and demise dates, seasonal length, and seasonal rainfall) of SouthEast Asian Summer Rainy Season (SEASuRS) from the 1001 ensemble members as:

$$\sigma_{noise}^2 = \frac{1}{K(N-1)} \sum_{k=1}^{K} \sum_{n=1}^{N} (A_{kn} - \bar{A}_n)^2 \quad ----------(1)$$

$$\sigma_{signal}^2 = \sigma_{em}^2 - \frac{1}{n}\sigma_{noise}^2 \quad ----------(2)$$

Where,

$$\sigma_{em}^2 = \frac{1}{(K-1)} \sum_{k=1}^{K} \left(\bar{A}_k - \bar{\bar{A}}\right)^2,$$

$$\bar{A}_k = \frac{1}{(N-1)} \sum_{n=1}^{N} A_{kn}, \text{ and}$$

$$\bar{\bar{A}} = \frac{1}{(K-1)} \sum_{k=1}^{K} \bar{A}_k$$

A could be anyone of onset date, demise date, seasonal length, and seasonal rainfall anomalies, k and n are indices for K years and N ensemble members, respectively.

The signal-to-noise ratio, SNR is then given by:

$$SNR = \frac{\sigma_{signal}^2}{\sigma_{noise}^2} \quad ----------(3)$$

When $SNR < 1$ signifies noise is dominant and when $SNR \gg 1$ then the signal dominates. A dominating signal suggests that the perturbations of the time-series will not significantly modulate the A diagnostic of the time-series.

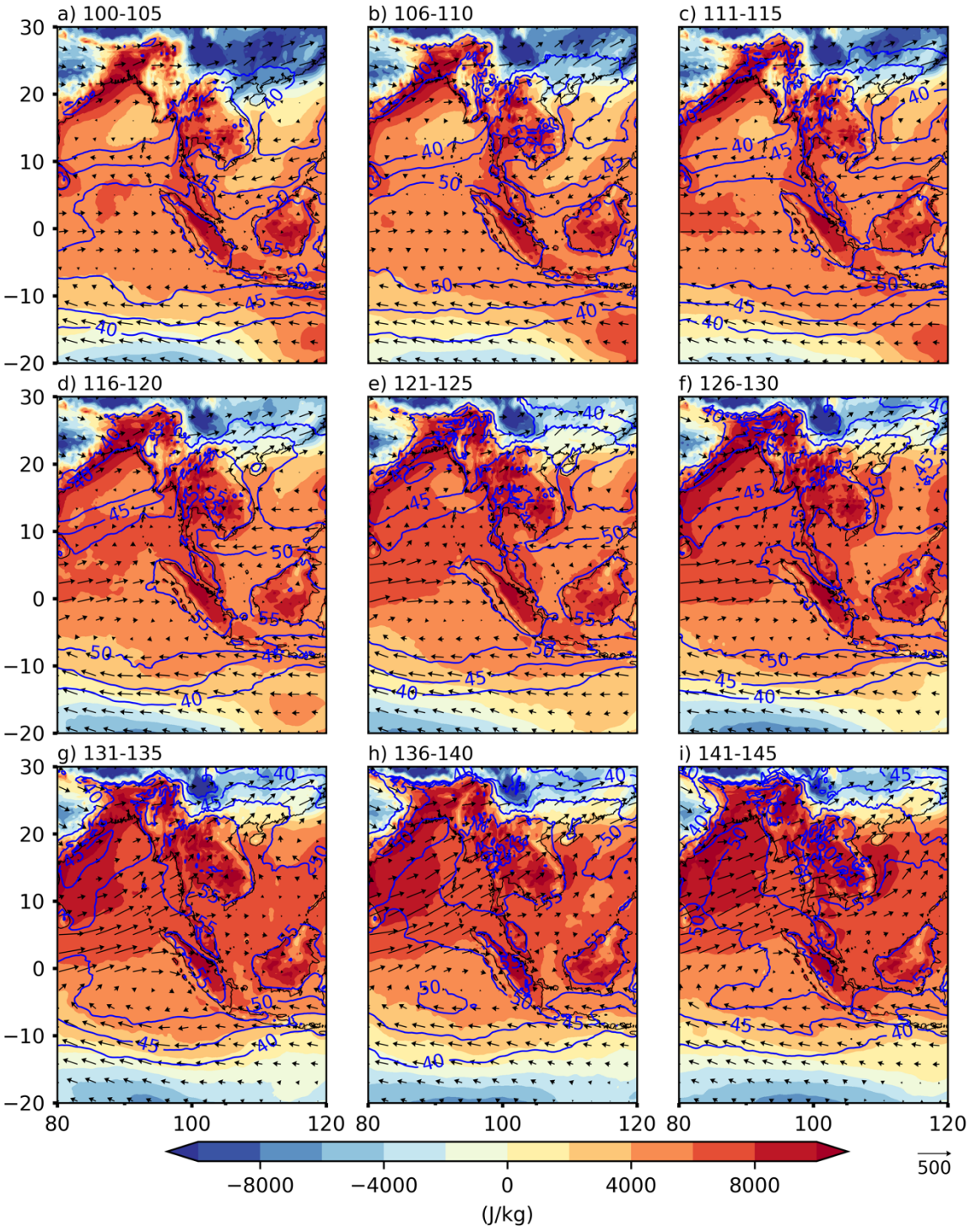

Figure S1: The climatological evolution of precipitable water (contour; units: mm) and vertically integrated moisture flux vectors (units: $kgm^{-1}s^{-1}$), and large-scale atmospheric stability (shaded; Jkg^{-1}) at intervals of 5 days from Julian Day 100 to 145 days.

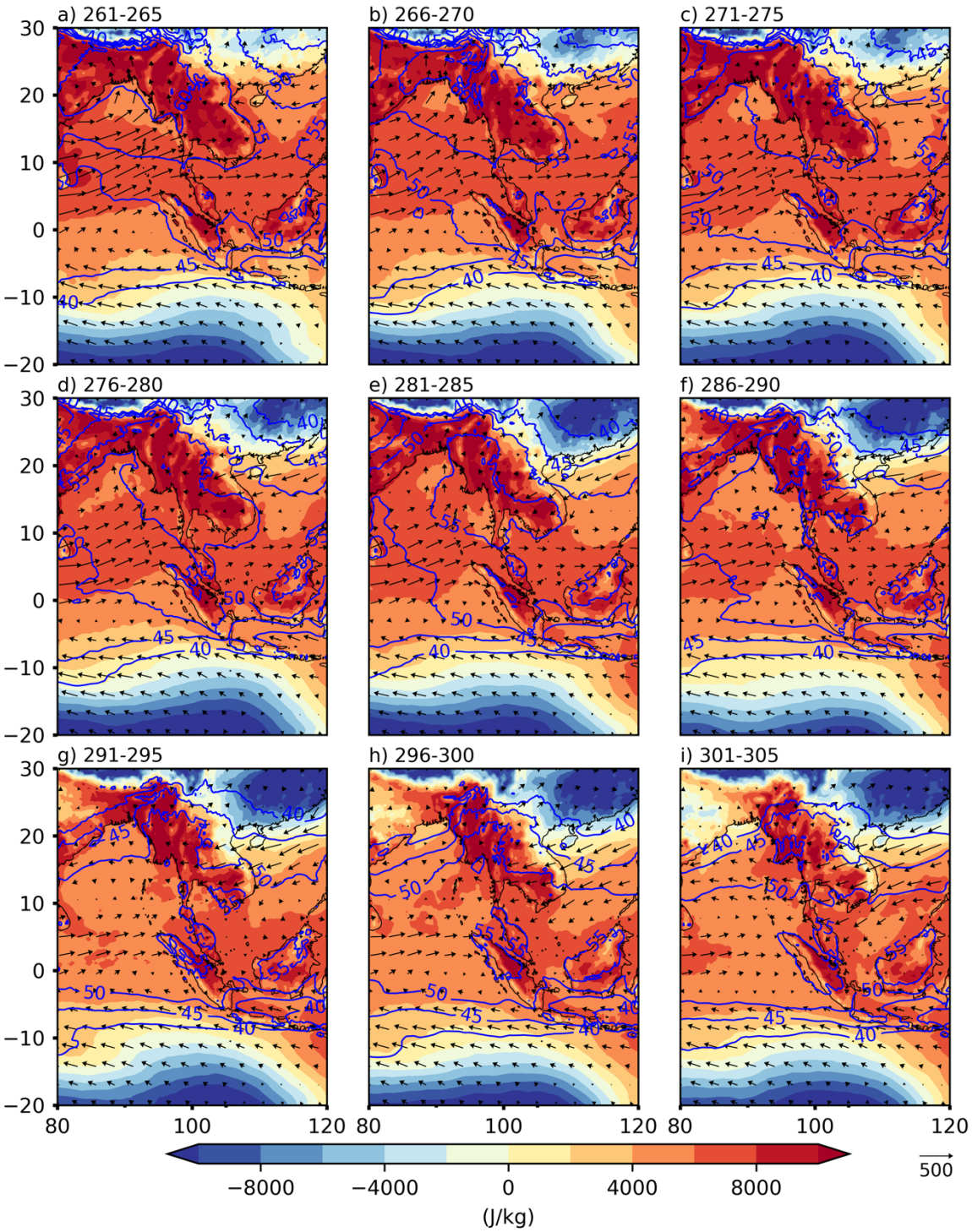

Figure S2: The climatological evolution of precipitable water (contour; units: mm) and vertically integrated moisture flux vectors (units: $kgm^{-1}s^{-1}$), and large-scale atmospheric stability (shaded; units: Jkg^{-1}) at intervals of 5 days from Julian Day 260 to 305 days.

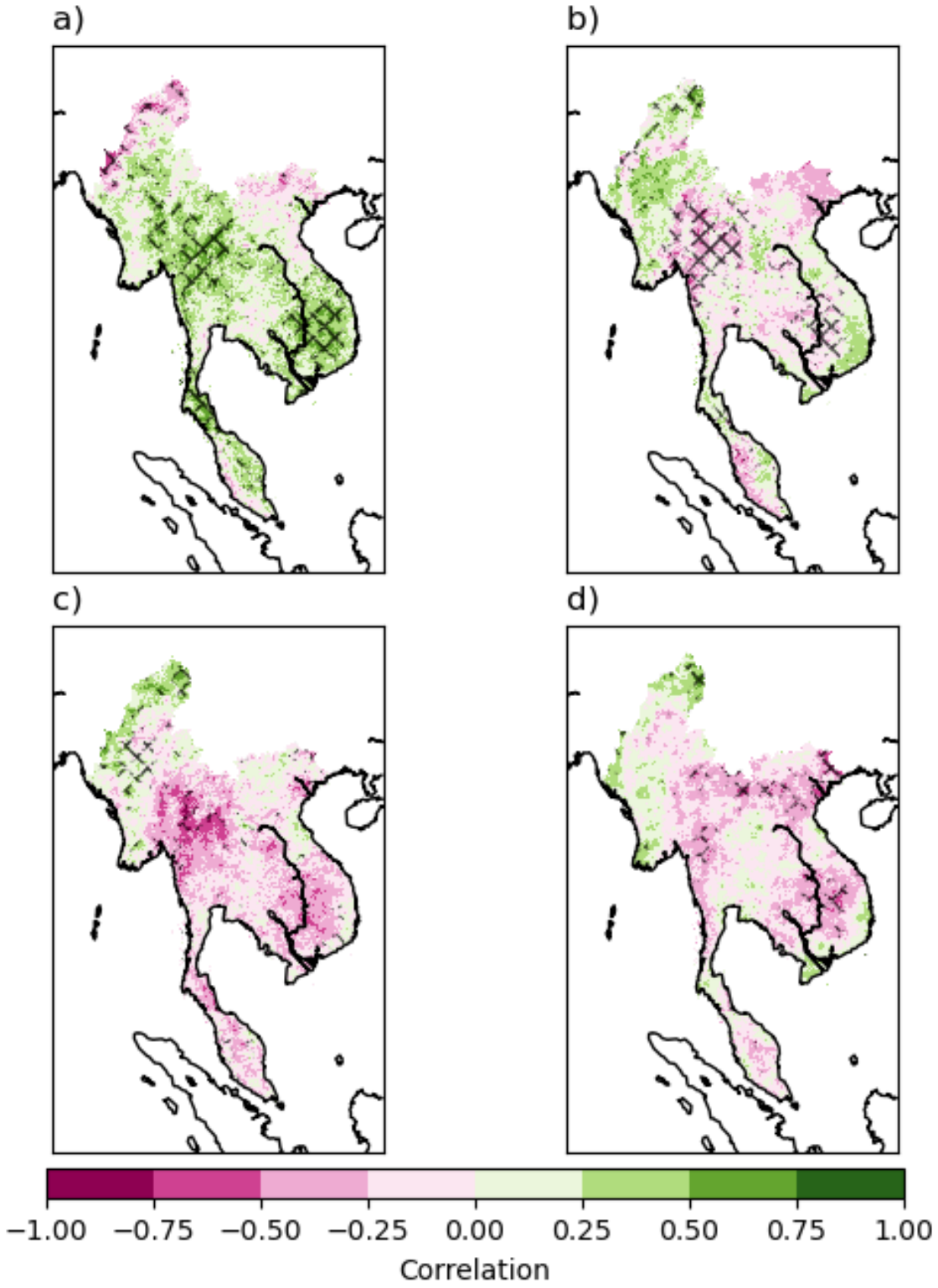

Figure S3: The correlation of preceding DJF Niño3.4 SST index with anomalies of (a) onset date, (b) demise date, (c) length, and (d) seasonal rain of the wet season. The crosshatching indicates statistical significance at 5% significance level following Student's t-test. However, all panels in this figure fail the Benjamini and Hochberg (1995) test.

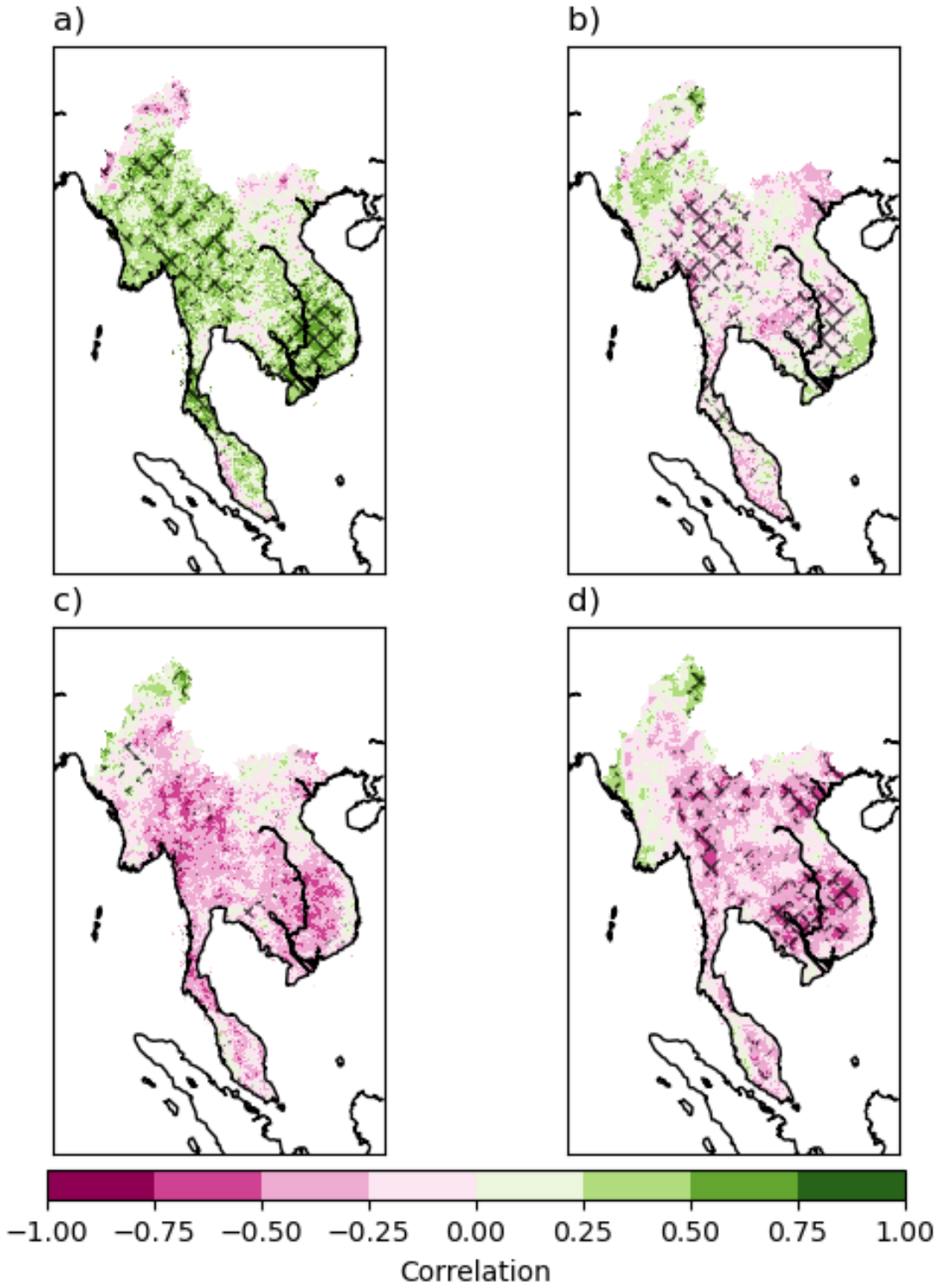

Figure S4: The correlation of preceding MAM Niño3.4 SST index with anomalies of (a) onset date, (b) demise date, (c) length, and (d) seasonal rain of the wet season. The crosshatching indicates statistical significance at 5% significance level following Student's t-test. However, all panels in this figure fail the Benjamini and Hochberg (1995) test.

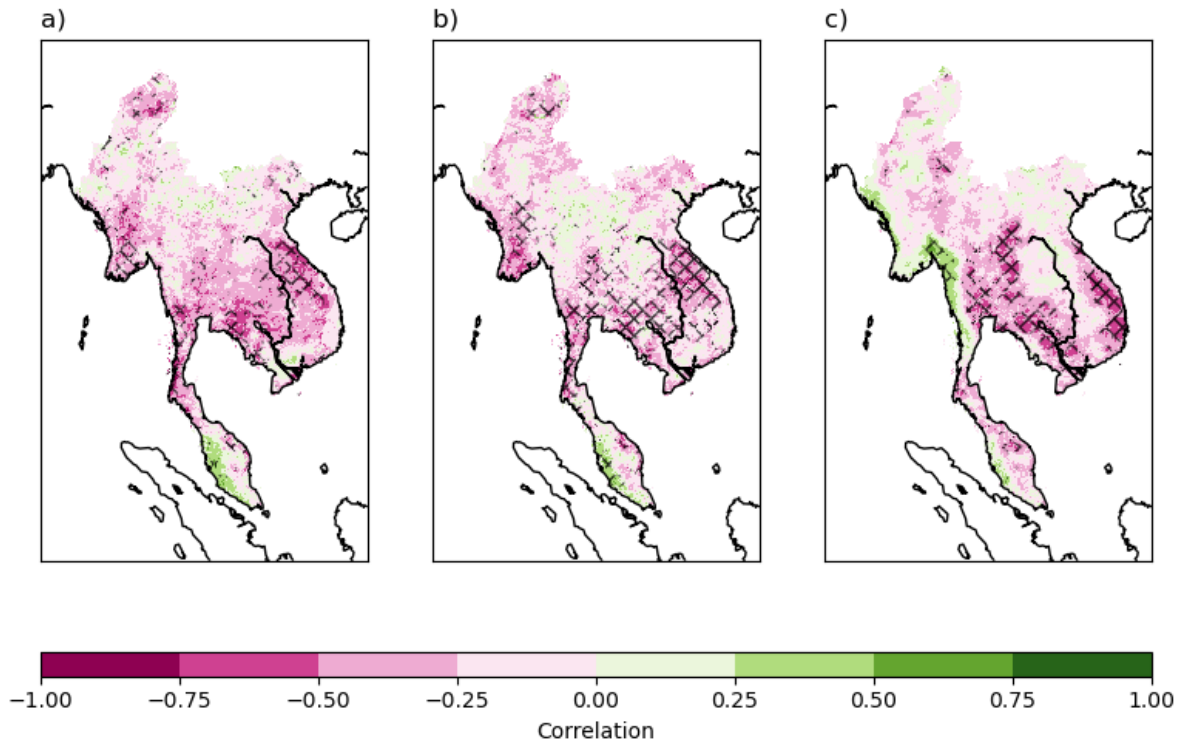

Figure S5: The correlation of contemporaneous SON IOD index with anomalies of (a) demise date, (b) length, and (c) seasonal rain of the wet season. The crosshatching indicates statistical significance at 5% significance level following Student's t-test. However, all panels in this figure fail the Benjamini and Hochberg (1995) test.

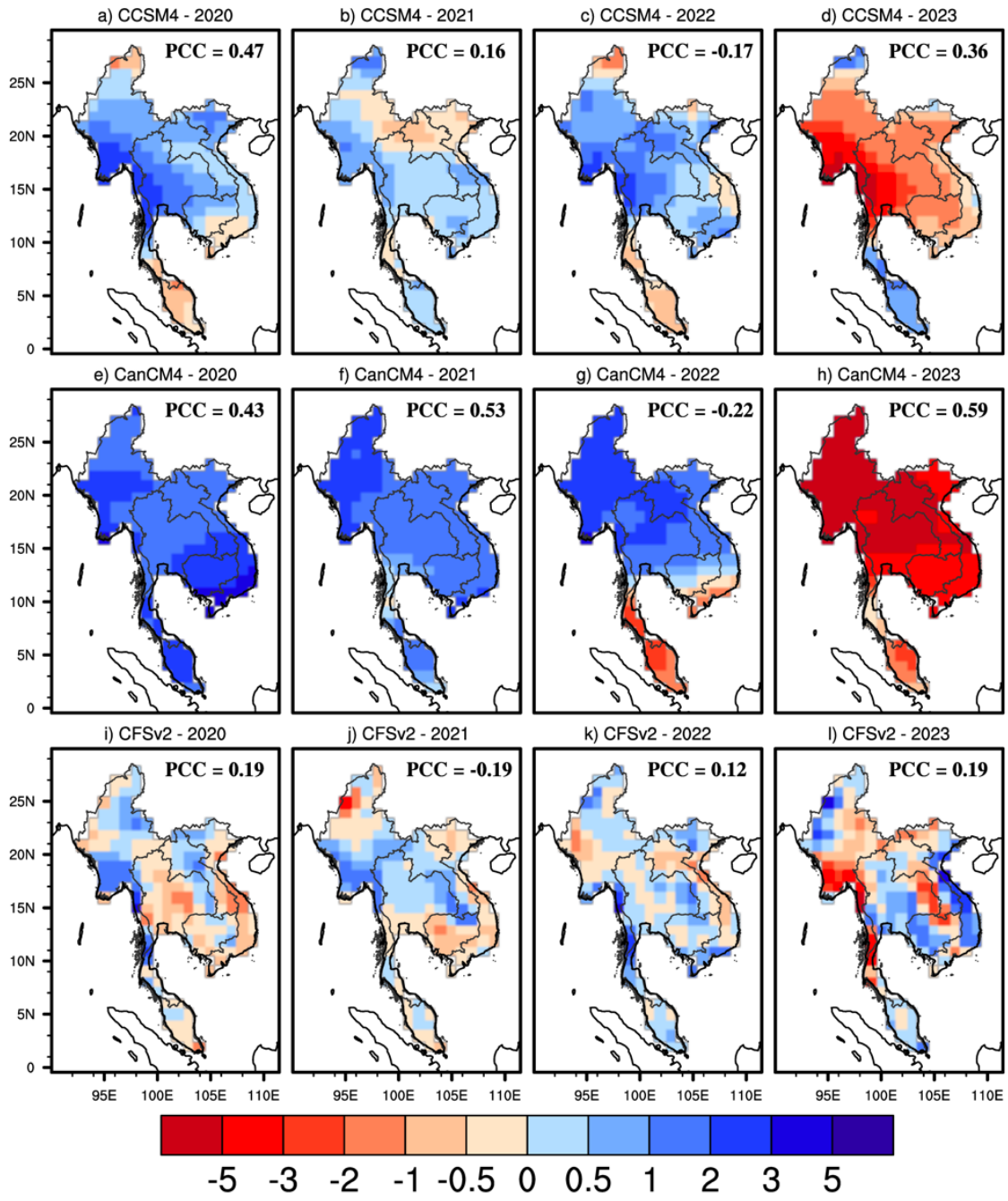

Figure S6: The seasonal mean precipitation anomalies (mm/day) for JJA from (a, b, c, d) CCSM4, (e, f, g, h) CanCM4, (i, j, k ,l) CFSv2 for (a, e, i) 2020, (b, f, j) 2021, (c, g, k) 2022, and (d, h, l) 2023. The pattern correlation coefficient (PCC) of each model with the corresponding IMERG seasonal anomalies are indicated in the top right corner of each panel.

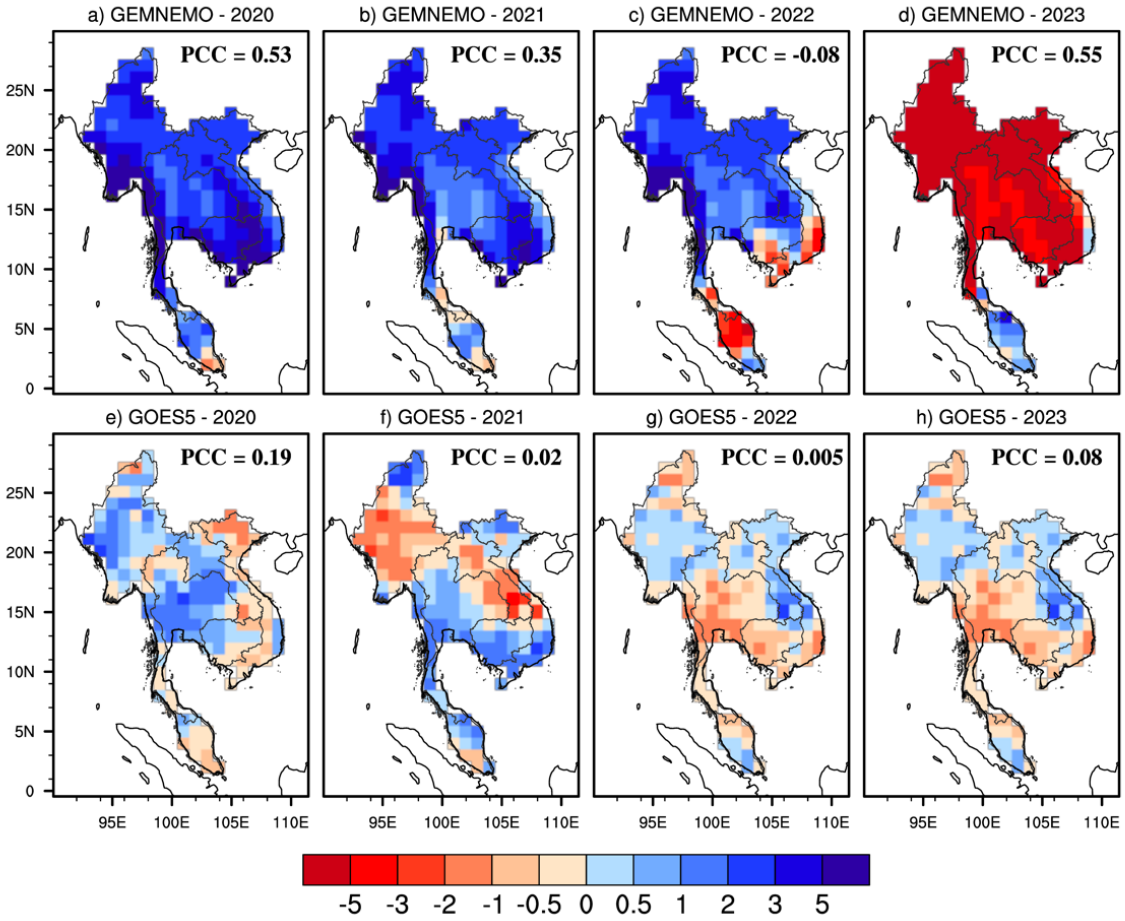

Figure S7: The seasonal mean precipitation anomalies (mm/day) for JJA from (a, b, c, d) GEMNEMO, (e, f, g, h) GOES5 for (a, e) 2020, (b, f) 2021, (c, g) 2022, and (d, h) 2023. The pattern correlation coefficient (PCC) of each model with the corresponding IMERG seasonal anomalies are indicated in the top right corner of each panel.

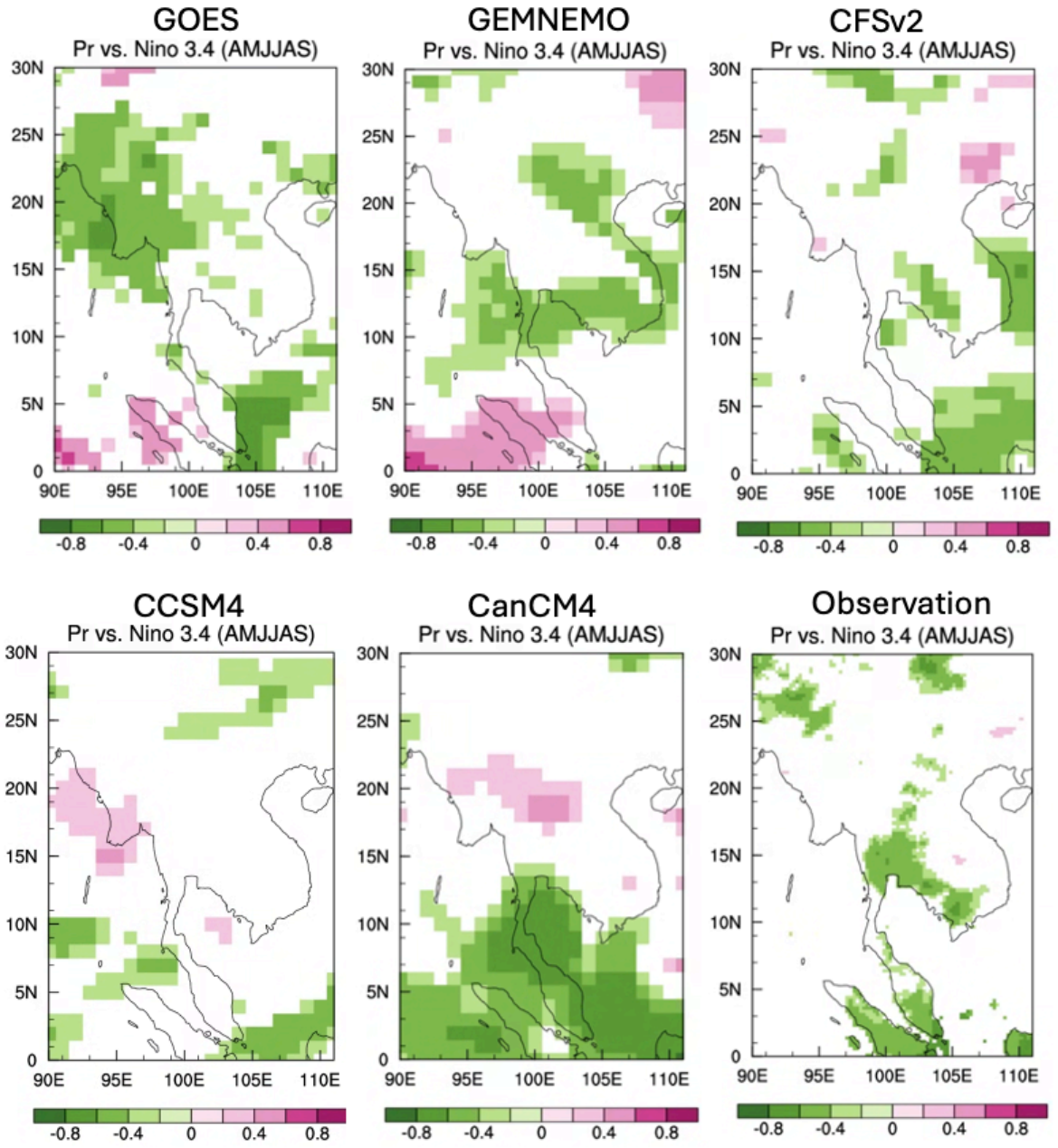

Figure S8: The contemporaneous correlations of April-September (AMJJAS) mean Niño3.4 SST index with corresponding rainfall anomalies from NMME models of (a) GEOS5, (b) GEMNEMO, (c) CFSv2, (d) CanCM4, and (e) CCSM4. (f) Similarly, contemporaneous correlations of April-September mean Niño3.4 SST index with corresponding rainfall anomalies from CHIRPS (Funk et al. 2015). The shading indicates statistical significance according to t-test at 10% significance level.